Supplementary Information for:

Nanoscale imaging reveals miRNA-mediated control of functional states of dendritic spines

Ikbum Park[a,1], Hyun Jin Kim[b,1], Youngkyu Kim[c,2], Hye Sung Hwang[b], Haruo Kasai[d], Joung-Hun Kim[b,3] and Joon Won Park[a,c,3]

[*]e-mail: joungkim@postech.ac.kr; jwpark@postech.ac.kr

This file includes:

SI Materials and Methods

References

Technical Comments on AFM imaging acquisition

Supplementary Figures 1–11

Supplementary Table 1

www.pnas.org/cgi/doi/10.1073/pnas.1819374116

SI Materials and Methods

AFM tip functionalization. Silicon nitride AFM tips (MSNL, Bruker, Santa Barbara, CA) were coated with 27-acid dendrons (custom synthesis, VRND NanobioOrganics, India) as described previously (1). Briefly, AFM tips were oxidized in a 10% nitric acid solution at 80°C for 20 min. The oxidized tips were silanized by reacting with *N*-(triethoxysilyl)-propyl-*O*-poly-(ethylene oxide) urethane (Gelest, Morrisville, PA) in a toluene solution (1.0% [v/v]) under nitrogen for 4 h and subsequent dehydration at 110°C for 30 min. The 27-acid dendrons were immobilized on the hydroxyl surface via the esterification of carboxylic groups of the dendrons in a dimethylformamide:dichloromethane (1:3 [v/v]) solution containing 1.0 mM 27-acid dendrons, 27 mM dicyclohexylcarbodiimide and 0.90 mM 4-dimethylaminopyridine for 12 h. Then, the protecting groups at the apexes of the immobilized dendrons were removed by treating with trifluoroacetic acid (1.0 M in dichloromethane) for 2 h.

The newly generated amine groups at the apexes were reacted with 4-maleimidobutyric acid *N*-hydroxysuccinimide ester (10 mM) in an acetonitrile solution containing 10 mM *N*,*N*-diisopropylethyl amine under nitrogen for 4 h. The AFM tips were placed in dimethylformamide with stirring for 20 min, rinsed with methanol and dried under a vacuum (30–40 mTorr). Subsequently, the tips were immersed in phosphate-buffered saline ([PBS] 10 mM phosphate, 2.7 mM KCl, 137 mM NaCl, pH 7.4) with glutathione (10 mM) for 4 h, rinsed thoroughly with deionized water (Milli-Q purification system, Millipore, Burlington, MA) and dried under vacuum.

The glutathione-immobilized tips were placed in PBS containing GST-fused HBD (200 nM) at room temperature for 2 h and rinsed with PBS with Tween 20 (0.05% [v/v]) and deionized water. The prepared tips were stored in PBS at 4°C and used within 1 week.

Neuronal cell cultures. Hippocampi were dissected from postnatal day 1 C57BL/6 mice and dissociated and cultured on poly-l-lysine-coated plates (Sigma, St. Louis, MO) or cover slips in Neurobasal medium (Invitrogen, Carlsbad, CA) supplemented with 2.0% B27 (Invitrogen), 1.0% GlutaMAX (Invitrogen), 2.0% fetal bovine serum (Welgene, South Korea), and 1.0% penicillin/streptomycin (Invitrogen) (v/v) in a humidified 5% CO_2/95% O_2 incubator at 37°C. After 6–8 h, the medium was replaced with serum-free conditioned neurobasal medium. After treatments, neurons were fixed at DIV14 with 4.0% formaldehyde in PBS (v/v) at 4°C for 15 min and then permeabilized with 0.20% Triton X-100 (Sigma) in PBS (v/v) at room temperature for 10 min or frozen as described below.

Preparation of neuronal sections by high-pressure freezing. To acutely freeze cells while preserving their membranes and cellular components, fixed cultured neurons were placed in a sample carrier within a high-pressure freezer (HPM 100; Leica, Germany). The frozen samples were kept in an EM AFS2 (Leica) chamber for substitution steps conducted as follows. The samples were kept in acetone for dehydration at -45°C for 1 day and embedded in Lowicryl HM20 resin (Electron Microscopy Sciences, Hatfield, PA) at -45°C for 2 days. The resin was polymerized under UV light for 1 day and then sectioned (300 nm) with an ultra-microtome (Leica). A series of sections of the neurons were placed on a glass slide. The sectioned neurons were permeabilized

with 0.50% Triton X-100 in PBS (v/v) at room temperature for 10 min before DNA hybridization was performed.

AFM-mediated categorization of dendritic spines. We employed the well-established classification parameters (such as spine length, head width, and neck width) established with the conventional imaging methods (2, 3) in order to categorize dendritic spines with AFM. AFM height images of filopodia and dendritic spines were analyzed using the JPK data processing program. All dendritic protrusions longer than 0.4 μm were considered for this analysis. Spine length was determined manually by measuring the maximal length of the entry from dendrite to the outermost part of the spine head. For spine width, a line was drawn across the widest part of the dendritic protrusion such as the spine head. Filopodia had lengths that were larger than the diameters of their neck and head, similar neck and head diameters, and protrusions less than 0.4 μm. Immature spines, such as thin-shaped spines, had lengths that were larger than their neck diameter. Mature spines had neck and head diameters that were similar to their lengths and the diameters of their heads were larger than those of their necks.

Marking of activated neurons using CaMPARI2. The construct pAAV_hsyn_NES-his-CaMPARI2-F391W-WPRE-SV40, which harbours an F391W mutation resulting in a high affinity for Ca^{2+} (K_d = 110 nM), was purchased from Addgene (plasmid #101061) and packaged into AAV according to an established protocol (4). Briefly, an equimolar mixture of helper plasmids, the pAAV-CaMPARI2 construct, and Lipofector Q transfection reagent (AptaBio, South Korea) was added to HEK-293T cells and incubated for 72 h. The transfected cells were lysed via multiple

freeze-thaw steps and the resultant viral particles were purified by iodixanol-gradient ultracentrifugation at 340,000 × *g* for 2 h. AAV particles were concentrated using an Amicon Filter tube (100K, Millipore) and virus titre (GC titre: 4.132×10^{11}) was determined by quantitative real-time PCR analysis (SYBR Green; Takara Bio Inc., Shiga, Japan). Cultured neurons were infected at DIV11 (0.5 µl virus/2 ml/chamber), and images were taken 3 days later, at DIV14, with a confocal microscope (Olympus, Japan) at 37°C in the presence of 0.5% CO_2. Cells were treated with BDNF- or BSA-coated beads (in 1 ml), and local fields were illuminated three times (duration, 10 s; interval, 5 s) with a 405 nm laser (PC light) through a 60× objective lens. Confocal images were obtained immediately after application of the beads and compared with those obtained after a contact time of 5 min. Lasers with wavelengths of 405 nm and 543 nm were used to visualize BSA beads and BDNF beads and CAMPARI2 signals, respectively. Montages of neuronal cell processes were captured by differential interference contrast (DIC) imaging.

Marking of active spines using ArcMin-AS. To visualize the active spines, the ArcMin-AS (5) construct was packaged into AAV according to an established protocol (4) to produce AAV2-SARE-ArcMin-PSDΔ1.2-mVenus-PaRac1-SV40 (GC titre: 6.812×10^{12}). Cultured neurons were infected (0.5 µl virus/2 ml media/chamber) at DIV11 and fixed 3 days later, at DIV14. mVenus fluorescence within neuronal dendrites and spines was captured by confocal microscopy and analyzed afterwards.

BDNF-coated beads and drug treatment. Bead preparation and usage for neuronal stimulation were as described previously (6). A PolyLink protein coupling kit (Polysciences, Warrington, PA)

utilizing carboxyl-EDAC [1-ethyl-3-(3-dimethylaminopropyl)-carbodiimide hydrochloride] was used to covalently immobilize recombinant human BDNF (R&D Systems, Minneapolis, MN) or BSA (Sigma) on 1.75 μm Fluoresbrite YO (Emission: 546 nm; no. 18449-10; Polysciences) or 1.0 μm Fluoresbrite BB (Emission: 407 nm; no. 17686-5; Polysciences) carboxylate microspheres, respectively. Briefly, the beads were pelleted for 10 min at 1,000 × *g* in a polypropylene tube (1.5 ml) at room temperature. PolyLink coupling buffer (400 μl, 50 mM MES [pH 5.2], 0.05% Proclin 300, Polysciences) was added to each pellet for washing, and the samples were centrifuged at 1,000 × *g* for 10 min; each pellet was resuspended in PolyLink coupling buffer (170 μl). An EDAC (Polysciences) solution was prepared by dissolving 10 mg EDAC in 50 μl PolyLink coupling buffer. The solution (20 μl) was added to the microbeads just before use, which were suspended by vortexing briefly. BDNF or BSA (500 ng) was dissolved in 1.0 ml PolyLink coupling buffer, and the protein solution was mixed with the above-prepared microbeads solution (190 μl) and incubated at room temperature for 1 hour with gentle shaking on a microplate shaker (PMS-1000i; Grant Instruments, UK). After pelleting the beads at 1,000 × *g* for 10 min and washing twice with 400 μl PolyLink wash/storage buffer (10 mM Tris-HCl [pH 8.0], 0.05% BSA, 0.05% Proclin 300, Polysciences) at room temperature, the beads were kept in 400 μl PolyLink storage buffer at 4°C. At DIV14, neurons were treated with a combination of BDNF- and BSA-coated beads for 1 h. The neuronal cells were fixed, and the beads were washed away prior to AFM imaging to avoid disrupting the movement of the cantilever during scanning. To block BDNF stimulation, the TrkB antagonist, ANA12, was bath-applied (10 μM, Tocris, UK) 10 min before either BDNF- or BSA-coated bead treatment.

DNA hybridization and immunocytochemistry. To avoid RNase contamination, experimental tools and glassware were treated with RNaseZap (Invitrogen) and ethanol, and deionized water was treated with diethyl pyrocarbonate (0.05% [v/v]) for 20 h and subsequently autoclaved. Permeabilized fixed neurons and frozen neuronal sections were incubated in a hybridization buffer (2× SSPE buffer [pH 7.4] with 7.0 mM SDS) containing the probe oligonucleotide (20 μM) at 34°C for 12 h. The cells/sections were sequentially washed for 15 min each in the hybridization buffer, 2× SSC buffer and 0.2× SSC buffer at 60°C with stirring.

For immunostaining, the cells/sectioned neurons were blocked with 10% normal goat serum (Gibco, MA) (in PBS [v/v]) at room temperature for 1 h, and labeled with mouse monoclonal antibody specific to MAP2A (MAB378, Millipore) (1:500 diluted in a blocking solution) at 4°C for 1 day. The hippocampal neurons were then incubated at room temperature for 90 mins with a goat anti-mouse secondary antibodies (Alexa 488-conjugated, A-11001 or Alexa 568-conjugated, and A-11004 for ArcMin-AS experiments only; Invitrogen) (1:500 diluted in a blocking solution). The prepared samples were immediately analyzed by AFM.

AFM experimentation and data analysis. A NanoWizard III AFM system (JPK Instruments, Germany) equipped with a fluorescence microscope (Axiovert 200, Zeiss, Germany) was used to image and map miR-134s. The spring constant of silicon nitride cantilevers was calibrated using a thermal fluctuation method, and the values ranged between 10 and 20 $pN \cdot nm^{-1}$. The AFM tips were placed on a sectioned neuronal somas or dendritic spines, and the morphology was imaged in QI mode before the commencement of force mapping. Adhesion force maps were acquired by recording force-distance curves five times per pixel with an approach/retraction speed of 3.0 $\mu m \cdot s^{-}$

[1] and a z-length of 500 nm. The maximum applied force was set at 80–100 pN to minimize mechanical damage. To observe the hydrodynamic radius of a miR-134/DNA hybrid, a pixel size of 4.0 nm was employed. To visualize individual hybrids in a larger area within a reasonable time span, the force maps were acquired at a pixel size of 10.0 nm. The collected force-distance curves were analyzed with the JPK data processing program and treated as described previously (1). Considering the observed hydrodynamic diameter (ca. 28 nm), a cluster of three connected pixels qualified as an individual miRNA.

Confocal microscopy. Laser scanning confocal microscope with a UPlansApo 60×/1.35 oil objective lens (FV1000, Olympus, Japan) was used to image primary cultured neuronal cells. Lasers with wavelengths of 488 and 543 nm were used to visualize mVenus and MAP2, respectively. Single focal plane images with a pixel size of 1024×1024 with a Confocal Aperture (C.A.) of 150 μm and digital zooms (5×, Fig S5 *A*; 3×, Fig S7 *A* and *B*; 4×, Fig S7 *D*).

References

1. Koo H, et al. (2016) Visualization and quantification of microRNA in a single cell using atomic force microscopy. *J Am Chem Soc* 138(36):11664–11671.6

2. Maiti P, Manna J, Ilavazhagan G, Rossignol J, Dunbar GL (2015) Molecular regulation of dendritic spine dynamics and their potential impact on synaptic plasticity and neurological diseases. *Neurosci Biobehav Rev* 59:208–237.

3. Schratt GM, et al. (2006) A brain-specific microRNA regulates dendritic spine development. *Nature* 439(7074):283–289.

4. Burova E, Ioffe E (2005) Chromatographic purification of recombinant adenoviral and adeno-associated viral vectors: methods and implications. *Gene Ther* 12:S5–S17.

5. Hayashi-Takagi A, et al. (2015) Labelling and optical erasure of synaptic memory traces in the motor cortex. *Nature* 525(7569):333–338.

6. Yoshii A, Constantine-Paton M (2007) BDNF induces transport of PSD-95 to dendrites through PI3K-AKT signaling after NMDA receptor activation. *Nat Neurosci* 10(6):702–711.

Technical Comments on AFM imaging acquisition

Over the past three decades, remarkable development and refinement in single molecule force spectroscopy has increased our ability to understand behavior of single molecules in biology. Atomic force microscopy (AFM) is one of the representative examples of the kind. AFM allowed for sensing molecular interactions at the picoNewton level, and it can be used in various conditions including vacuum and under physiological conditions. In particular, AFM would merit assessment of specific molecules at the area of interest at the nanometric spatial resolution.

As summarized in Figure S1, the first step is acquiring fluorescence and morphology images and then identifying spine types. The second step is obtaining force maps (1×1 μm^2 for each) at a selected spine region by using a HBD tethering tip. Finally, the maps are combined to cover the whole area of the spine, and the combined force and the morphology maps are overlaid. Typically, more than five force maps were obtained to cover the whole area of a spine. Because it takes about 5 hrs for each map, and it is required to sort 50,000 FD force curves and retrieve force values from them, the procedure is time-consuming. However, little variation of the copy number was observed among different fixed samples even with the lengthy scanning time. The small variation supported that the sampling number (at least 5) used in the study was sufficient to elucidate the change among spines at different stages.

Various new instruments for AFM hold promises to get the force and morphology maps further rapidly. Therefore, it is expected to visualize the whole body of a single cell in a reasonable time frame soon with such progress. Together with a data analysis program, the tool and current approach should be useful for scientists in neuroscience and related areas.

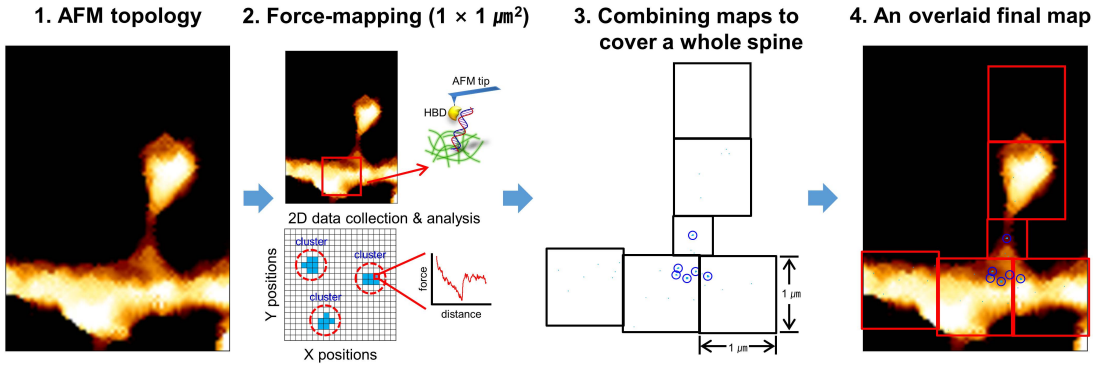

Figure S1. An overall scheme for the AFM imaging steps.

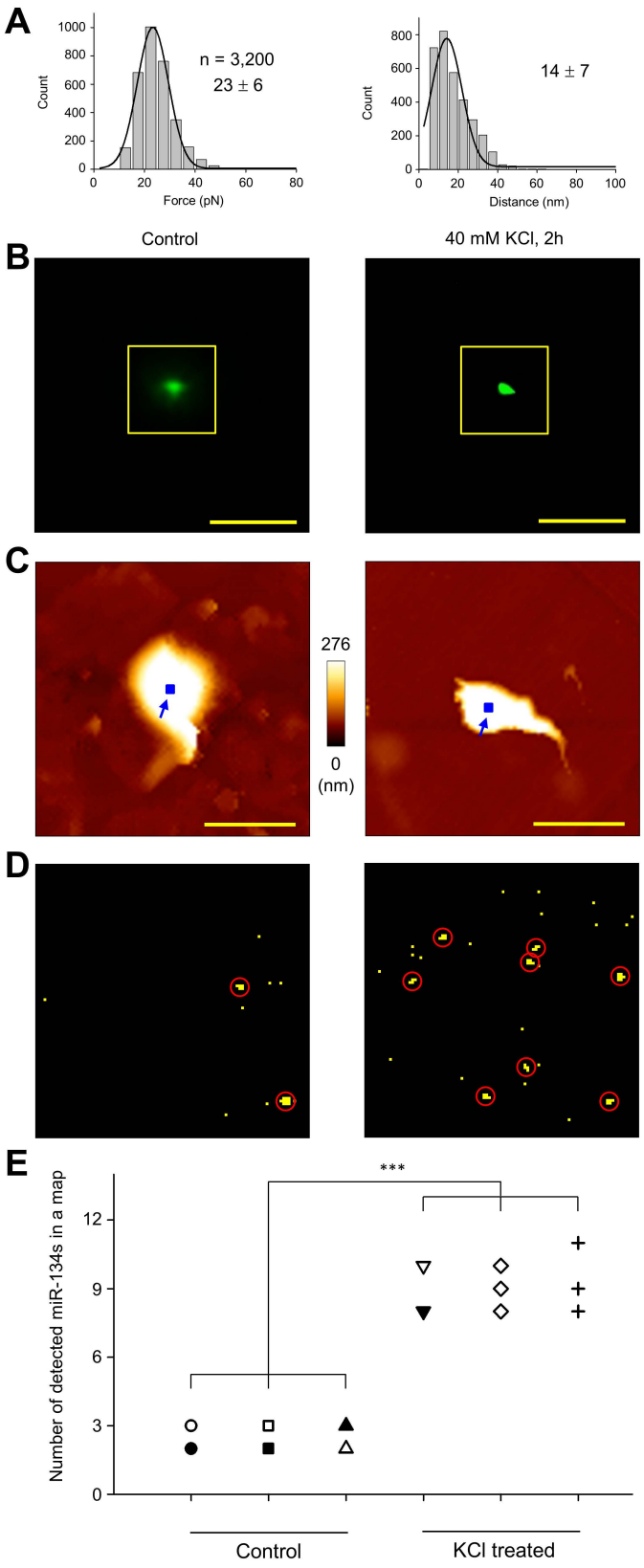
A
n = 3,200
23 ± 6
Count
Force (pN)
14 ± 7
Distance (nm)
B
Control
40 mM KCl, 2h
C
276
0
(nm)
D
E
***
Number of detected miR-134s in a map
Control
KCl treated

Figure S2. Visualization of miR-134s at sectioned soma. (*A*) Histograms of the adhesion force (*Left*) and tip-sample distance (*Right*) for the unbinding events; *n* indicates the number of curves analysed to generate the histogram. The most probable values are given as the mean ± s.d. from the Gaussian fit. (*B*) Primary hippocampal neurons were stimulated with 40 mM KCl for 2 h, fixed, sectioned after high-pressure freezing and then immunostained for MAP2. (*C*) Boxed region in *B* was imaged with AFM. Scale bars: 30 μm (*B*), 10 μm (*C*). (*D*) Three arbitrary positions on the sectioned soma were examined with force mapping, examples are marked as blue arrows in *C* (100 × 100 pixels, 1.0 × 1.0 μm^2). The yellow pixel represents a location where specific unbinding events were observed in more than two out of five measurements (pixel size, 10 nm), and a red circle indicates a cluster corresponding to the hydrodynamic radius observed at high resolution (qualified clusters). (*E*) Three regions were examined for a single soma (filled symbols represent overlapped data points), and three cells were examined under the same conditions. $^{***}P < 0.001$ via one-way ANOVA followed by a post hoc Tukey's test shows the difference between the pristine neurons and the stimulated ones is significant.

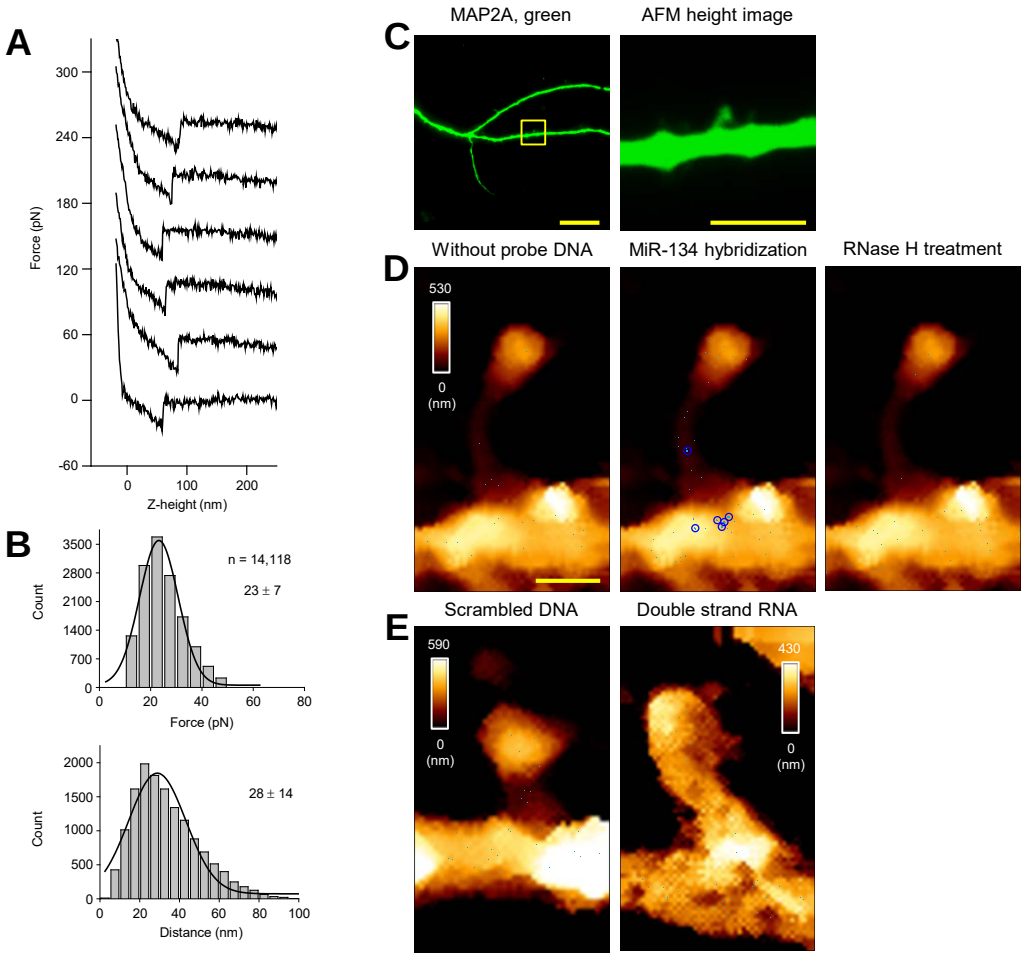

Figure S3. Control experiments to verify the specificity of the observed miR-134. (*A*) Unbinding events for the adhesion between HBD and miR-134/DNA hybrid of dendritic spines. (*B*) Histograms of the adhesion force (top) and tip-sample distance for the unbinding events (bottom). *n* indicates the number of curves analysed to generate the histogram. The most probable values are given as the mean ± s.d. from the Gaussian fit. (*C*) Fluorescence images of the mature spine (DIV14); the boxed area (*Left*) is shown at higher magnification (*Right*); MAP2; green. (*D*) Topology of the spine in the boxed area was obtained with AFM (3.0×5.0 μm^2), and the force maps were obtained before (*Left*) and after (*Middle*) hybridization with miR-134 complementary DNA. The same region was re-scanned after RNase H treatment (*Right*) with the same tip. The clusters representing miR-134 appeared and disappeared. (*E*) Scrambled DNA (22-nt) for miR-134 (*Left*) and miR-134 complementary RNA (*Right*) were applied, and no cluster was observed. A sky-blue pixel represents a location where specific unbinding events were observed in more than

two out of five measurements (pixel size, 10 nm), and blue circle indicates a cluster corresponding to the hydrodynamic radius observed at high resolution. Scale bars: 20 μm (*C*, *Left*), 5.0 μm (*C*, *Right*), 1.0 μm (*D*). The scale bar for the AFM maps in *D* and *E* is same as that of the first corresponding map.

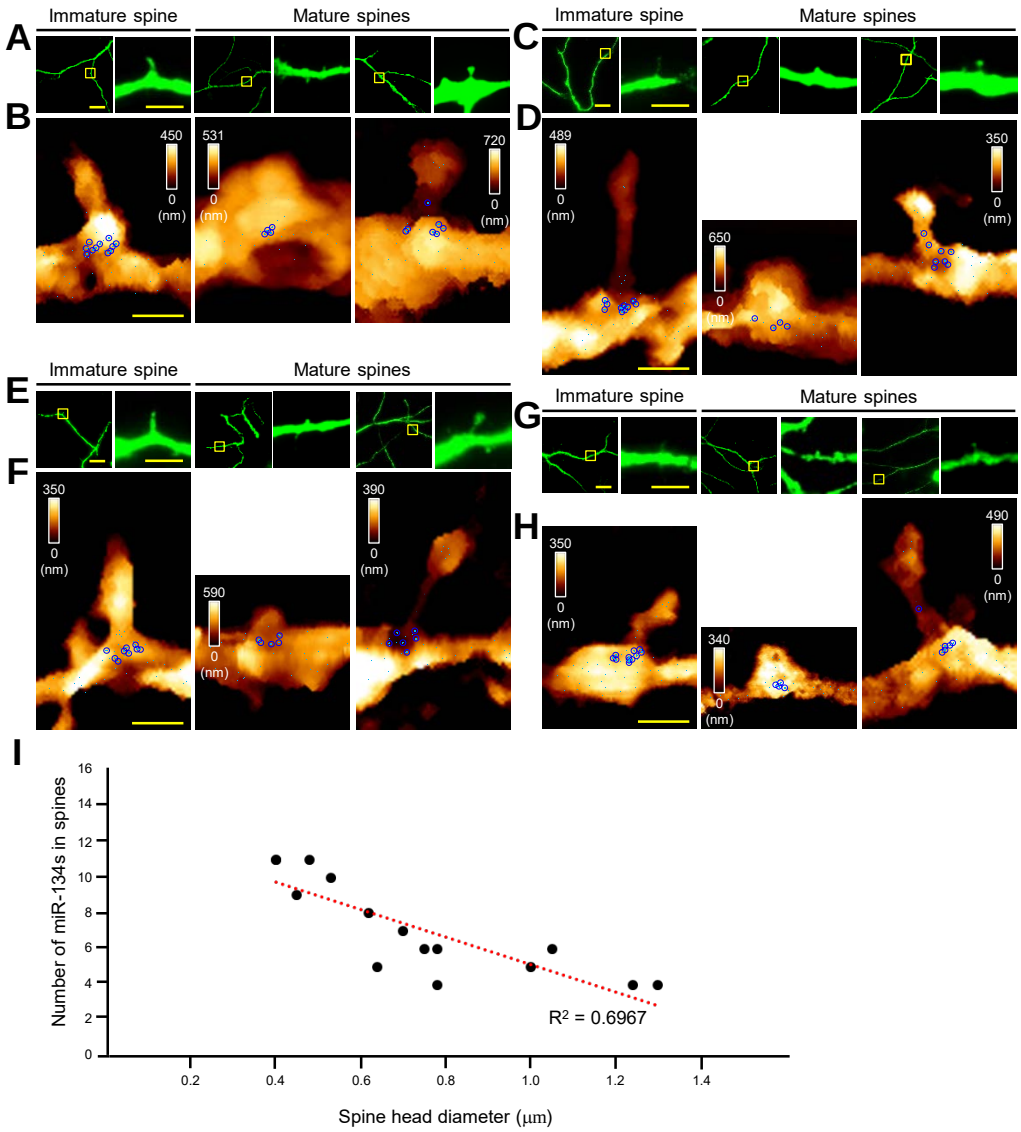

Class	Spine 1	Spine 2	Spine 3	Spine 4	Spine 5	Spine 6	Spine 7	Spine 8	Spine 9	Spine 10	Spine 11	Spine 12	Spine 13	Spine 14	Spine 15
head size (μm)	1.05	0.78	0.75	0.7	0.62	1.3	1.0	0.78	1.24	0.64	0.40	0.40	0.53	0.48	0.45
miR-134s	6	6	6	7	8	4	5	4	4	5	11	11	10	11	9

Figure S4. Visualization of individual miR-134s associated with various dendritic spines and their correlations. (*A*, *C*, *E*, *G*) Fluorescence images showing immature and mature spines (DIV14); the boxed area (*Left*) is shown at higher magnification (*Right*); MAP2, green. (*B*, *D*, *F*, *H*) AFM topographic images and overlaid force maps of the boxed areas in *A*, *C*, *E* and *G*. A sky-blue pixel represents a location where specific unbinding events were observed in more than two out of five measurements (pixel size, 10 nm), and blue circle indicates a cluster corresponding to the hydrodynamic radius observed at high resolution. (*I*) A negative correlation between the

number of observed miR-134s in spine (Y axis) and spine head diameter (X axis) (Kendall *tau* correlation coefficient: -0.76; $P < 0.001$). Below table indicates raw data of the scattered plot. Scale bars: 20 μm (*A, C, E* and *G*, left image for each pair), 5.0 μm (*A, C, E* and *G*, right image for each pair), 1.0 μm (*B, D, F* and *H*). The scale bar for the fluorescence images in *A, C, E* and *G* is the same as that in the first corresponding image, and the scale bar for the AFM maps in *B, D, F* and *H* is the same as that in the first corresponding map.

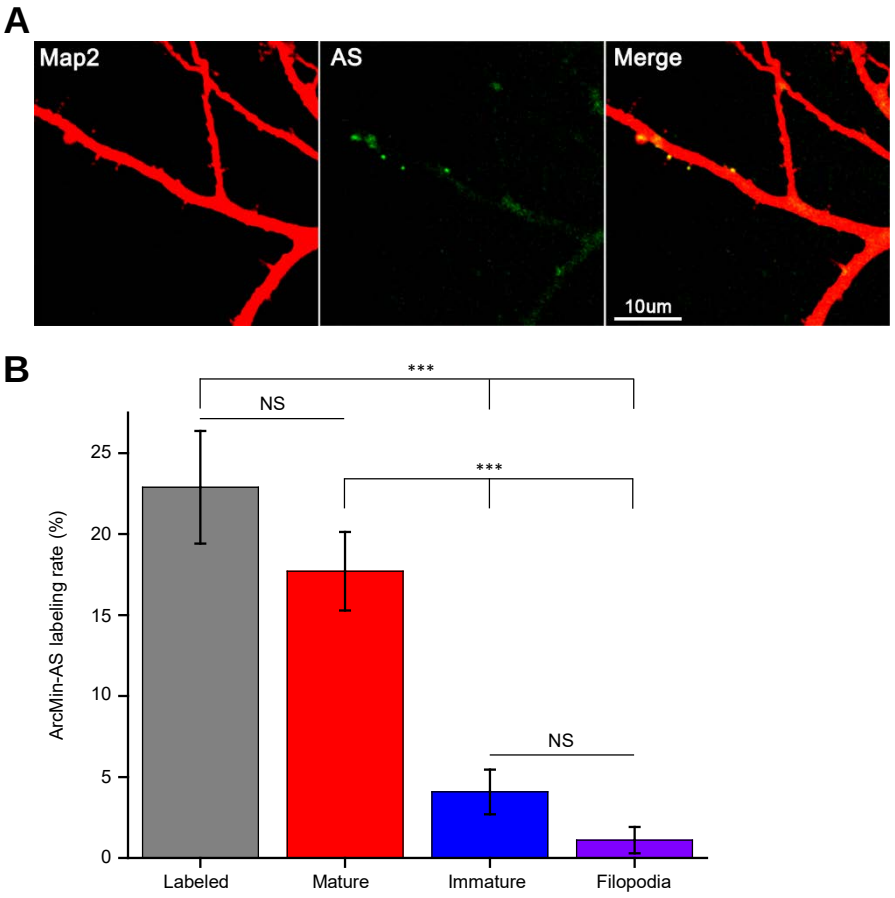

Figure S5. Confocal microscopy of filopodia and dendritic spines probed with ArcMin-AS. (*A*) Fluorescence images of filopodia and dendritic spines (DIV14); dendritic marking with MAP2, red; activity marking with ArcMin-AS, green. Active filopodia and spines appear yellow in the merged image. (*B*) Labelling rate of ArcMin-AS in filopodia and dendritic spines. 22.89% of filopodia and spines were activated under spontaneous stimulation, of which 17.71% were mature and 4.08% immature types of spine, and 1.10% were filopodia. $^{***}P < 0.001$ via one-way ANOVA followed by a Tukey's post hoc test; NS, not significant.

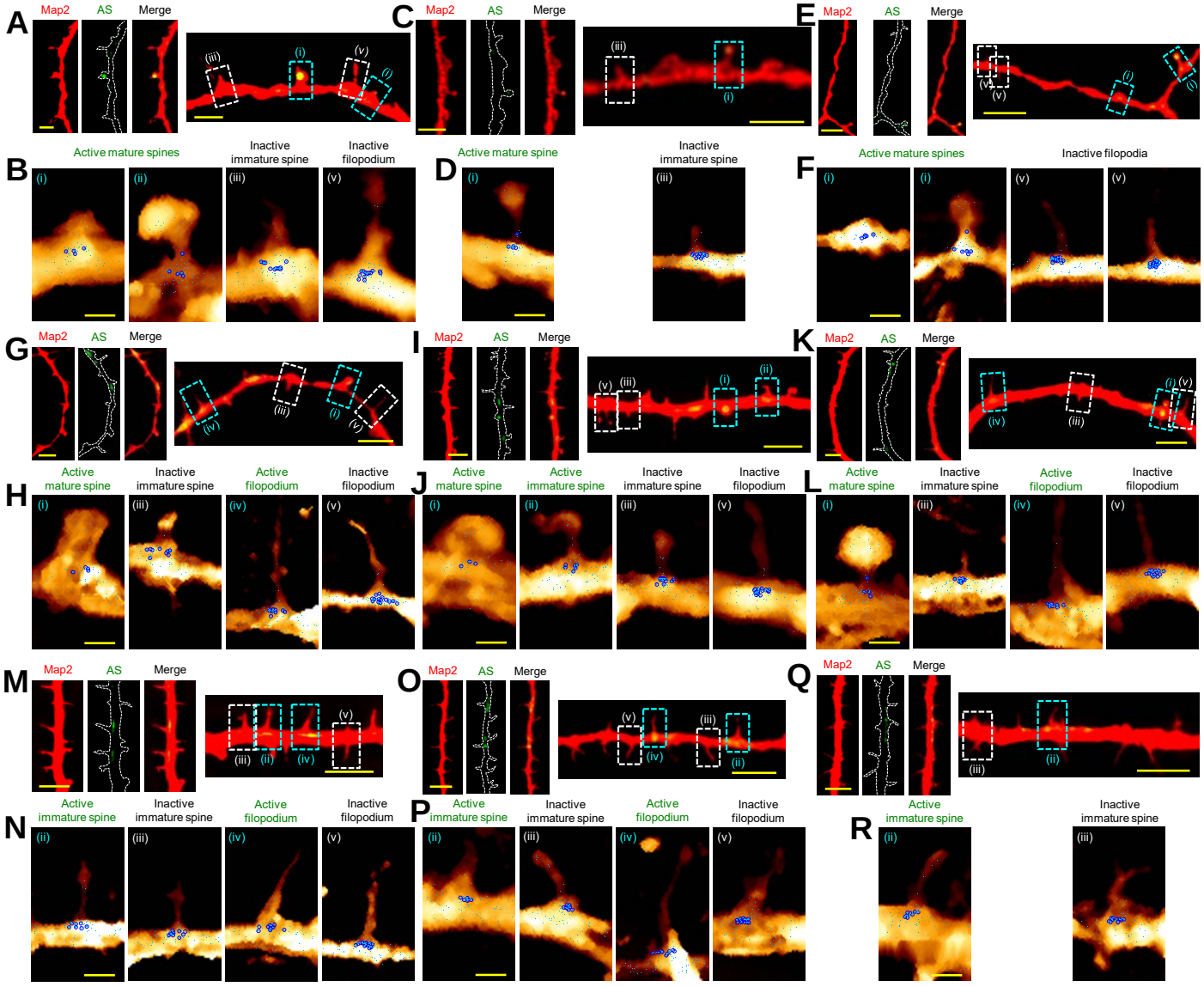

Figure S6. Mapping of miR-134s at spontaneously-active and inactive filopodia and dendritic spines labelled with ArcMin-AS. (*A, C, E, G, I, K, M, O, Q*) Fluorescence images of filopodia and dendritic spines (DIV 14); AS, ArcMin-AS. Active mature (i) and immature spine (ii) and filopodium (iv) and an inactive immature spine (iii) and filopodium (v). (*B, D, F, H, J, L, N, P, R*) AFM topographic images and force maps were obtained for the boxed areas *A, C, E, G, I, K, M, O* and *Q*. Scale bars: 20 μm (*A, C, E, G, I, K, M, O* and *Q*, left images in each set), 5.0 μm (*A, C, E, G, I, K, M, O* and *Q*, right images in each set), 1.0 μm (*B, D, F, H, J, L, N, P* and *R*). The scale bar for the AFM maps in *B, D, F, H, J, L, N, P* and *R* is the same as that in the first corresponding map.

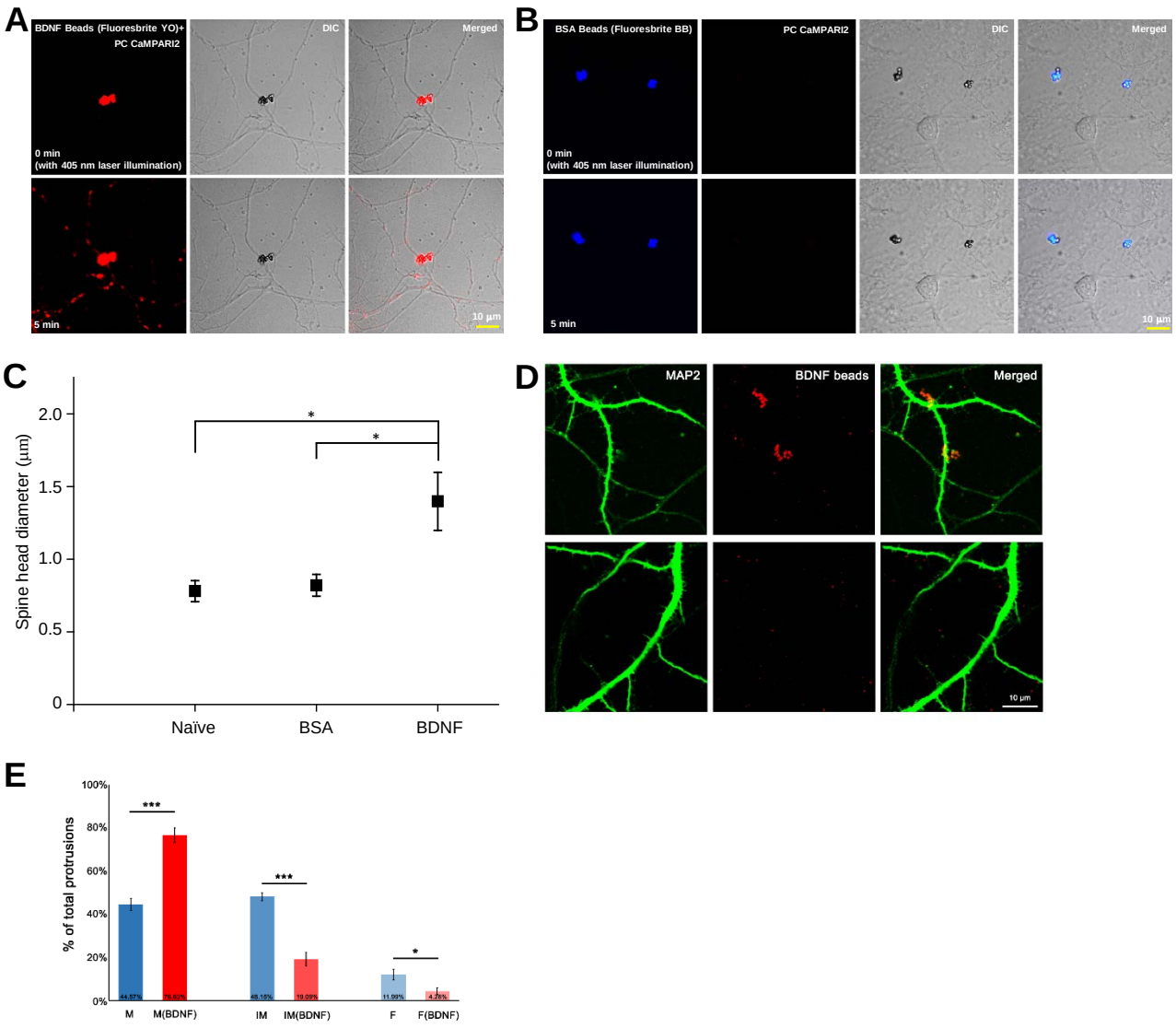

Figure S7. Validation of local activation by BDNF beads. (*A*) Immediately after the treatment with BDNF-coated beads (first row), no photoconverted (PC) CaMPARI2 signal was detected, and only beads (Fluoresbrite YO, 546 nm) were visible on the dendrites; 5 min later (second row), the CaMPARI2 signals were evident. (*B*) Immediately after the treatment with BSA-coated beads (Fluoresbrite BB, 407 nm) and 5 min later (second row), the CaMPARI2 signal was not detected on the dendrites. Scale bar: 10 μm. (*C*) Mature spine head enlargement induced by BDNF-coated beads (Naïve, 0.78 ± 0.07; BSA-coated beads, 0.82 ± 0.08; BDNF-coated beads, 1.40 ± 0.20 μm; $n = 5$). One-way ANOVA followed by a post hoc Tukey's test shows $^{*}P < 0.05$. (*D*) Representative images for dendrites with or without contact of BDNF beads. First row images for dendrites with BDNF-coated beads and second row for dendrites without BDNF-coated beads. (*E*) Proportion of

mature type (*M*) of spines significantly increased, whereas that of immature type (IM) of spines and filopodia (*F*) decreased with application of BDNF-coated beads (dendrites un-bound to BDNF-coated beads, n = 8; dendrites bound to BDNF-coated beads, n = 9; two tailed *t*-test, $^{***}P < 0.001$, $^{*}P < 0.05$).

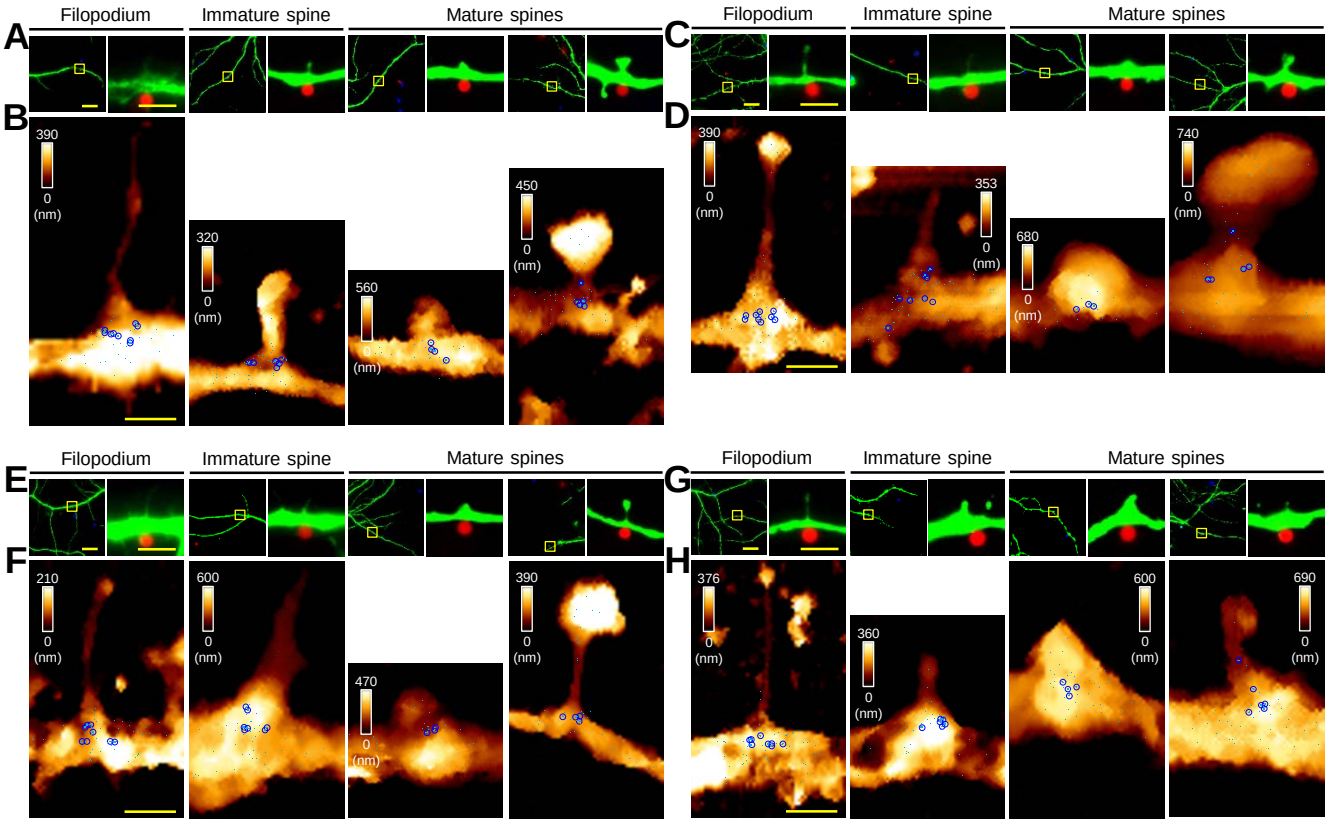

Figure S8. Mapping of miR-134s at filopodia and dendritic spines locally stimulated by BDNF-coated beads. (*A, C, E, G*) Fluorescence images of filopodia and immature and mature spines (DIV14). The images on the right show the boxed areas in the left panels at higher magnification, in which a BDNF-coated bead (in red) can be seen to make contact with the dendrite (MAP2, green). (*B, D, F, H*) AFM topographic images of the boxed areas in panels *A, C, E* and *G* overlaid with the force maps for stimulated filopodia and spines. A sky-blue pixel represents a location where specific unbinding events were observed in more than two out of five measurements (pixel size, 10 nm), and the blue circle indicates a cluster corresponding to the hydrodynamic radius observed at the high resolution. Scale bars: 20 μm (*A, C, E* and *G*, left image for each pair), 5.0 μm (*A, C, E* and *G*, right image for each pair), 1.0 μm (*B, D, F* and *H*). The scale bar for the fluorescence images in *A, C, E* and *G* is the same as that of the first corresponding image, and the scale bar for the AFM maps in *B, D, F* and *H* is the same as that of the first corresponding map.

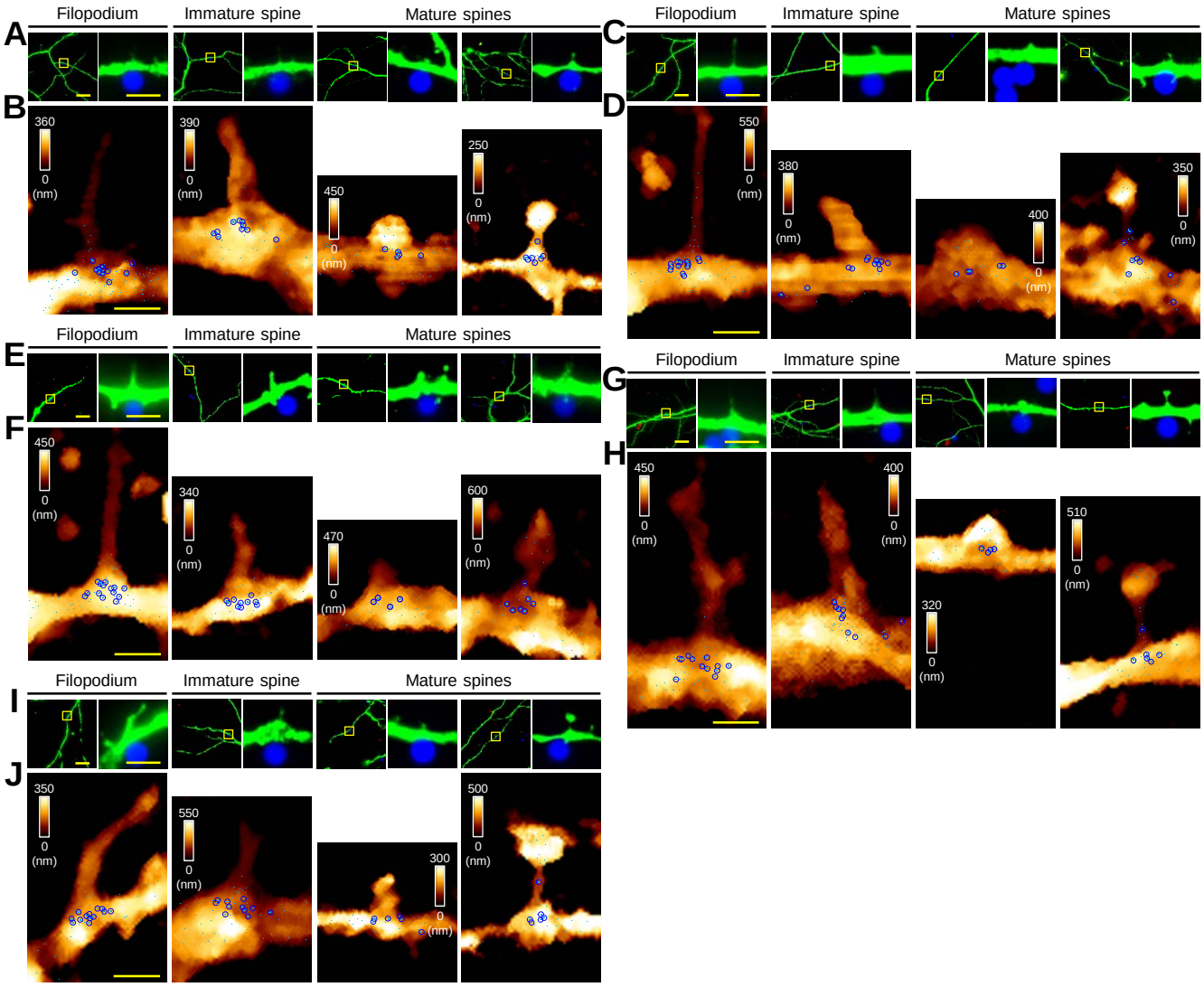

Figure S9. Mapping of miR-134s at filopodia and dendritic spines in contact with BSA-coated beads. (*A, C, E, G, I*) Fluorescence images of filopodia, immature and mature spines (DIV14). The images on the right show the boxed areas in the left panels at higher magnification, in which a BSA-coated bead (in blue) can be seen to make contact with the dendrite (MAP2, green). (*B, D, F, H, J*) AFM topographic images of the boxed areas in panels *A, C, E, G* and *I* overlaid with the force maps for BSA beads in contact with filopodia and spines. A sky-blue pixel represents a location where specific unbinding events were observed in more than two out of five measurements (pixel size, 10 nm), and blue circle indicates a cluster corresponding to the hydrodynamic radius observed at the high resolution. Scale bars: 20 μm (*A, C, E, G* and *I*, left image for each pair), 5.0 μm (*A, C, E, G* and *I*, right image for each pair), 1.0 μm (*B, D, F, H* and *J*). The scale bar for the fluorescence images in *A, C, E, G* and *I* is the same as that of the first

corresponding image, and the scale bar for AFM maps in *B, D, F, H* and *J* is the same as that of the first corresponding map.

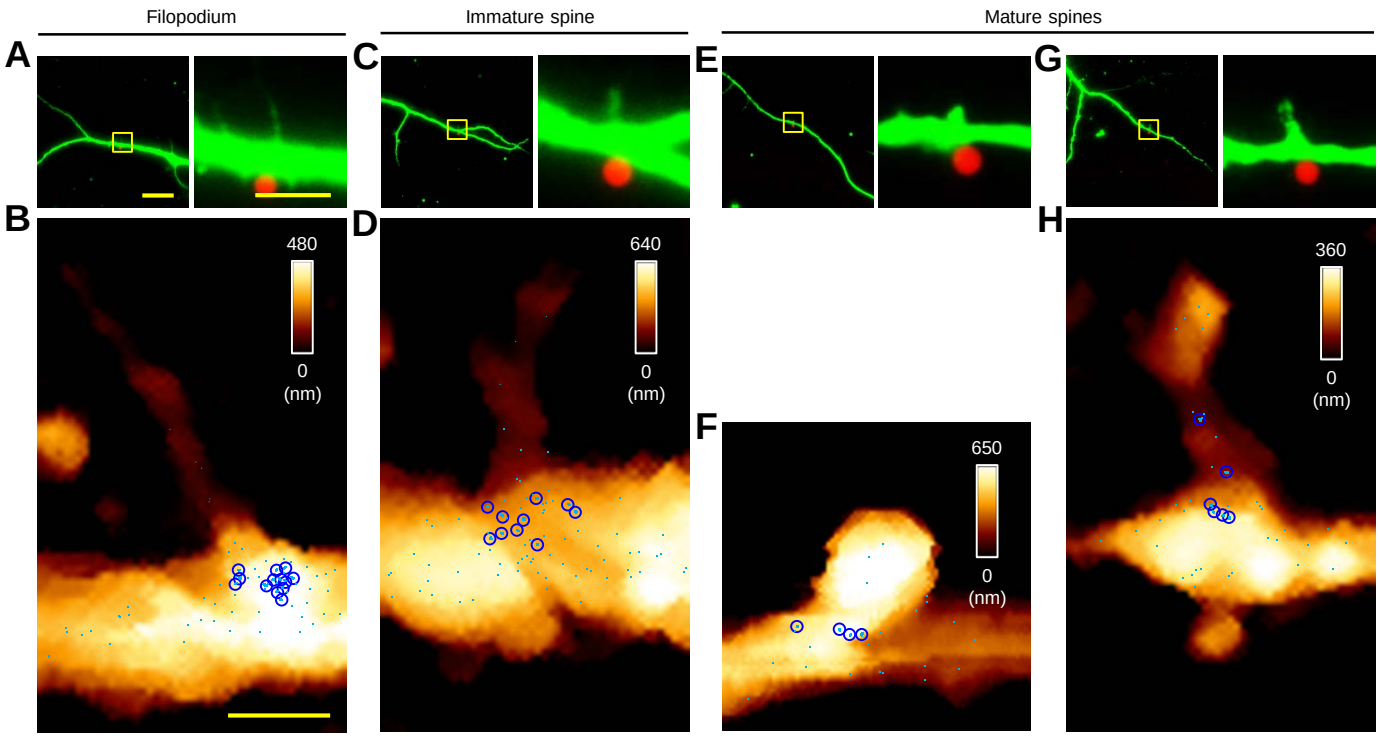

Figure S10. Block the BDNF stimuli by ANA-12 treatment. (*A*) Fluorescence images of a filopodium (DIV14); the boxed area (*Left*) is shown at higher magnification (*Right*), where a BDNF-coated bead (in red) is seen in contact with a dendrite (MAP2, green). (*B*) AFM topographic image of the boxed area in *A* (3.0×5.0 μm^2) overlaid with the force map for an ANA-12-treated filopodium. (*C*) Fluorescence image of an immature spine. (*D*) AFM topographic image of the boxed area in *C* (3.0×5.0 μm^2) overlaid with force map for an ANA-12-treated immature spine. (*E*, *G*) Fluorescence images of mature spines. (*F*, *H*) AFM topographic images of the boxed area in *E* and *G* (3.0×3.0 μm^2 or 3.0×5.0 μm^2) overlaid with force maps for ANA-12-treated mature spines. A sky-blue pixel represents a location where specific unbinding events were observed in more than two out of five measurements (pixel size, 10 nm), and blue circle indicates a cluster corresponding to the hydrodynamic radius observed at high resolution. Scale bars: 20 μm (*A*, *Left*), 5.0 μm (*A*, *Right*), 1.0 μm (*B*). The scale bar for the fluorescence images in *C*, *E* and *G* is the same as that of the corresponding image in *A*, and the scale bar for AFM maps in *D*, *F* and *H* is the same as that of the corresponding map in *B*.

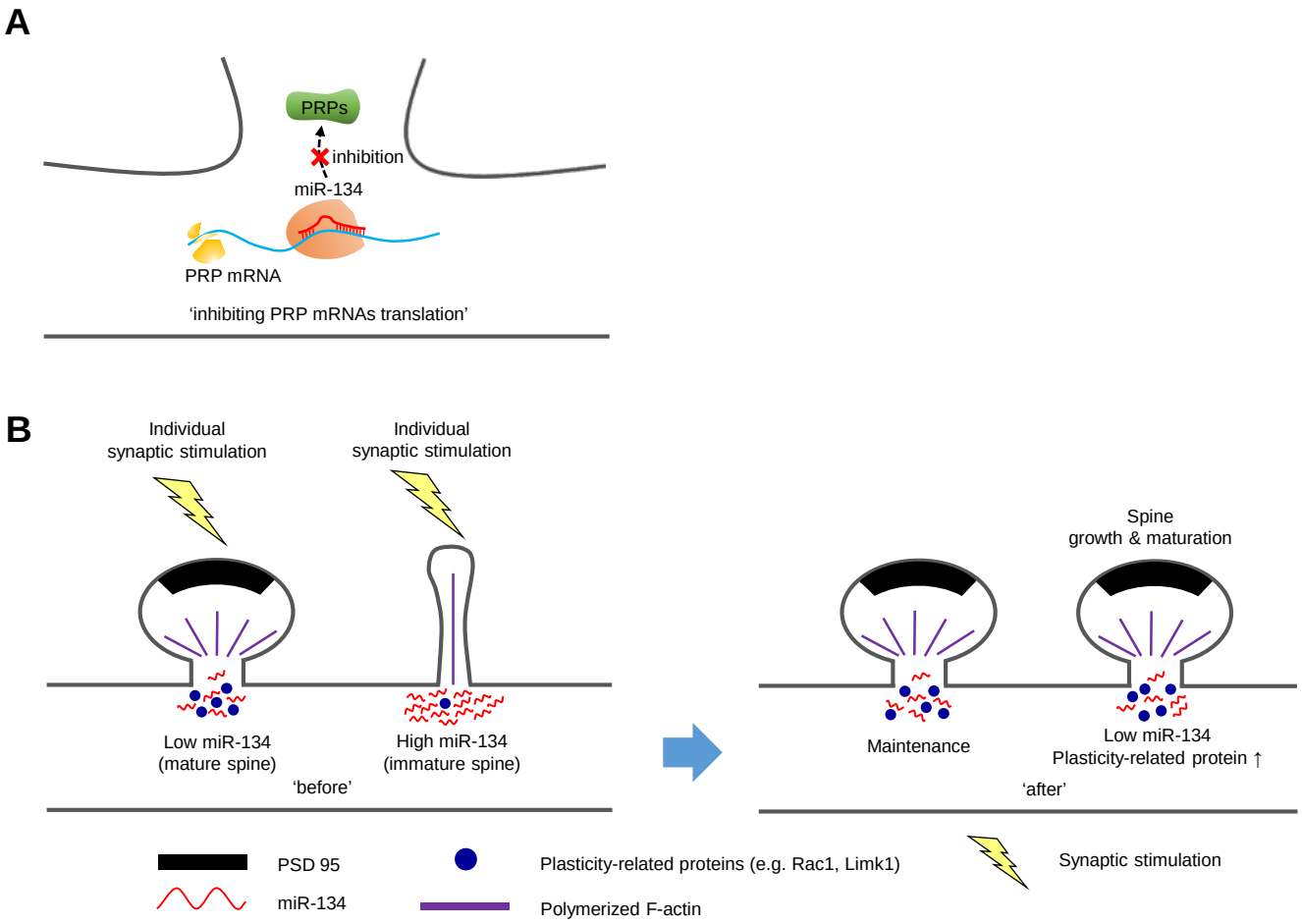

Figure S11. Simplified models for miR-134-mediated regulation of dendritic spines. miR-134s are distinctly localized at the base of dendritic spines and likely regulate spine structures. (*A*) miR-134s basally inhibit translation of plasticity-related protein (PRP) mRNAs, thereby restricting spine growth or maturation. (*B*) Immature forms of spines at rest have a high level of miR-134s, which limits synthesis of PRPs (e.g., Rac1, Limk1). At spontaneously active spines or spines stimulated with BDNF or other inputs, miR-134 repression is relieved, which triggers production of PRPs and enhanced actin polymerization for spine growth and maturation.

Observed number of miR-134s in a spine												
Naïve	Class	Spine 1	Spine 2	Spine 3	Spine 4	Spine 5	Spine 6	Spine 7	Spine 8	Spine 9	Spine 10	Mean ± SEM
	M	6	6	8	7	6	5	4	4	4	5	5.50 ± 0.43
(N=5, n=15)	IM	11	11	10	11	9						10.40 ± 0.40
	Class	Spine 1	Spine 2	Spine 3	Spine 4	Spine 5	Spine 6	Spine 7	Spine 8	Spine 9	Spine 10	Mean ± SEM
BDNF	M	5	5	5	4	6	4	4	3	3	4	4.30 ± 0.30
(N=6, n=20)	IM	6	6	8	7	6						6.60 ± 0.40
	F	8	9	9	8	8						8.40 ± 0.24
	Class	Spine 1	Spine 2	Spine 3	Spine 4	Spine 5	Spine 6	Spine 7	Spine 8	Spine 9	Spine 10	Mean ± SEM
BSA	M	7	8	6	7	6	5	5	4	4	6	5.80 ± 0.42
(N=4, n=20)	IM	10	12	10	10	11						10.60 ± 0.40
	F	12	13	12	14	13						12.80 ± 0.37
ArcMin-AS	Class	Spine 1	Spine 2	Spine 3	Spine 4	Spine 5	Spine 6	Spine 7	Spine 8	Spine 9	Spine 10	Mean ± SEM
(Active)	M	5	5	6	6	4	4	5	5	4	3	4.70 ± 0.30
	IM	6	7	7	6	8						6.80 ± 0.37
(N=6, n=11)	F	10	9	9	8	8						8.80 ± 0.37
ArcMin-AS	Class	Spine 1	Spine 2	Spine 3	Spine 4	Spine 5	Spine 6	Spine 7	Spine 8	Spine 9	Spine 10	Mean ± SEM
(Inactive)	IM	10	11	11	9	10	9	11	10	9	10	10.00 ± 0.26
(N=6, n=11)	F	13	15	14	14	14	14	13	13	15	12	13.70 ± 0.30

Table S1. Numbers of miR-134 clusters associated with naïve (control) spines, filopodia and spines with BDNF bead stimulation, filopodia and spines with BSA bead contact, spontaneously active filopodia and spines (probed by ArcMin-AS), and inactive filopodia and dendritic spines. The mean and standard error of the mean (SEM) values for each class of spines and filopodia were calculated. Mature spines were collected from 10 spines of individual cells and immature spines and filopodia were collected from 5 spines of individual cells, and ArcMin-AS labelled (activated) or un-labelled (inactivated) spines or filopodia were collected from 11 dendritic segments of individual cells. M, mature spine; IM, immature spine; F, filopodium.